19th Australasian Fluid Mechanics Conference
Melbourne, Australia
8-11 December 2014

Advances in Probability Density Function Methods for Turbulent Reactive Flows

S.B. Pope[1] **and R. Tirunagari**[1]

[1]Sibley School of Mechanical & Aerospace Engineering
Cornell University, Ithaca, New York 14853, U.S.A.

Abstract

In Probability Density Function (PDF) methods applied to turbulent flows, a modeled transport equation is solved for the joint PDF of the fluid properties. Three recent studies are reviewed in which the composition PDF method is used in conjunction with a Large-Eddy Simulation (LES) to make calculations of turbulent flames for which there are experimental data. These are: a temporal non-premixed jet flame exhibiting local extinction and re-ignition; a bluff-body stabilized premixed flame; and, a premixed opposed jet flame. These calculations demonstrate the capabilities of the method to account for challenging turbulence-chemistry interactions. PDF methods are also used in the context of Reynolds-Averaged Navier-Stokes (RANS) modeling, and two contributions are described to the development and testing of the PDF sub-models used. It is shown that the principal (tensor) coefficient in the Generalized Langevin Model (GLM) for velocity is directly related to the conditional mean fluid acceleration, and that it can be extracted from measurements of the velocity-acceleration correlations. Second, a new method is proposed for testing the Shadow-Position Mixing Model (SPMM).

Introduction

This paper describes recent advances in PDF methods for turbulent reactive flows—that is, modeling and simulation approaches based on a modeled transport equation for the joint probability density function (PDF) of fluid properties. These PDF methods are used both in the context of Reynolds-Averaged Navier-Stokes (RANS) and in conjunction with Large-Eddy Simulations (LES). Recent reviews of PDF methods in both contexts are provided in [9, 16].

In the next section we review recent LES/PDF simulations performed at Cornell, which are for three qualitatively different turbulent flames [27, 11]. Then, in the following two sections, we review two recent developments in PDF modeling in the RANS context, namely: an improved understanding of the underlying Generalized Langevin Model (GLM) [17]; and, the shadow-position mixing model [15], to model the effects of molecular mixing.

Recent LES/PDF Simulations

The LES/PDF simulations described in the following three subsections are based on the same models and codes. The low Mach number, finite-difference LES code NGA [3] is used to solve the mass and momentum conservation equations for the resolved velocity, and also for the specific volume (i.e., the inverse of the resolved density). The particle/mesh code HPDF [26] solves the modeled transport equation for the joint PDF of the fluid composition (i.e., the species specific moles and sensible enthalpy). Using the algorithm described in [18], the PDF code provides the specific volume and its rate of change to the LES code.

The dynamic Smagorinsky model [6] is used to determine the residual stresses, and the IEM mixing model [24] is implemented using the algorithm described in [25], which allows differential diffusion to be accounted for.

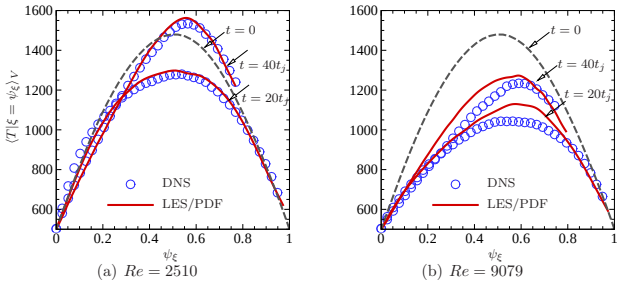

(a) $Re = 2510$ (b) $Re = 9079$

Figure 1: Temperature (K) conditional on mixture fraction ψ_ξ in the temporal jet flame at $Re = 2,510$ (left) and $Re = 9,079$ (right) at $t/t_j = 20$ and 40. Symbols, DNS [7]; Solid lines, LES/PDF [27]; Dashed line, $t/t_j = 0$. (From [27])

Temporally-Evolving Non-Premixed Jet Flame

In [27], LES/PDF calculations are reported for the temporal jet flame studied using direct numerical simulation (DNS) by Hawkes *et al.* [7]. At the initial time (t=0), there is a slab of thickness H of fuel composed of $CO/H_2/N_2$ (50/10/40 by volume) moving to the right at speed $U/2$, on both sides of which there is oxidant O_2/N_2 (25/75 by volume) moving to the left at speed $U/2$. The interface between the fuel and oxidant is specified according to a laminar flame profile. The DNS use detailed, molecular transport and an 11-species chemical mechanism. Two Reynolds numbers (based on U, H, and the viscosity of the fuel) are studied, $Re = 2,510$ and $Re = 9,079$. Time in the simulation is measured relative to the reference time $t_j \equiv H/U$.

As time evolves, turbulence is generated in the shear layers separating the fuel from the oxidant, and reaction and mixing take place. A principal finding in the DNS study is that (by design) there is significant local extinction around $t/t_j = 20$, more so at the higher Reynolds number, and this is followed by reignition. This is evident in figure 1, which shows the conditional mean temperature, conditional on the mixture fraction. As may also be seen from the figure, the LES/PDF calculations quite accurately represent both the extinction (evidenced by the depressed temperatures at $t/t_j = 20$) as well as the reignition.

Bluff-Body Stabilized Premixed Flame

In [11], the same LES/PDF methodology is applied to a premixed flame, stabilized on a triangular flame-holder in a square duct, which has been studied experimentally by Sjunnesson *et al.* [20]. Figure 2 shows a sketch of the flow and a visualization of the flame obtained from an instantaneous field of the resolved mass fraction of CO. The flame-holder height is $h = 4cm$, and the duct's square cross-section is $4h \times 4h$. The nominally uniform stream (upstream of the flame-holder) is premixed propane/air, with an equivalence ratio of 0.6, at a temperature of $600K$, and a velocity of $34m/s$.

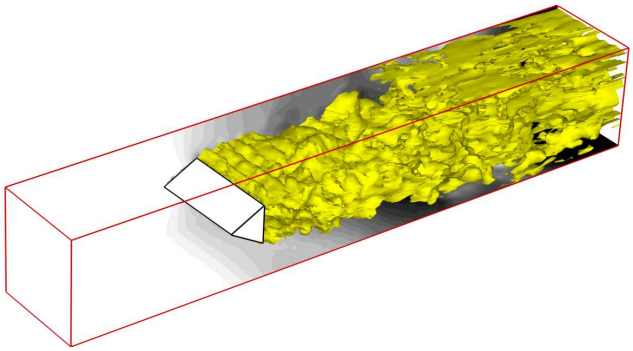

Figure 2: Instantaneous constant-property surface $Y_{CO} = 0.003$ from LES/PDF calculations [11] of the "Volvo" premixed flame [20]. (From [11])

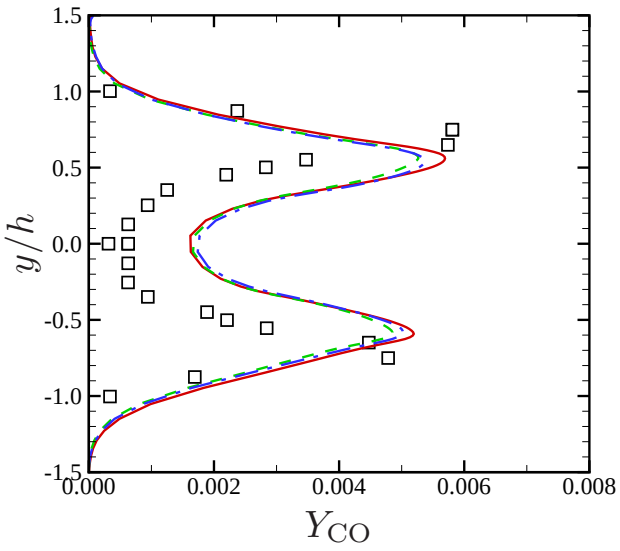

Figure 3: Lateral profiles of the mean mass fraction of CO at an axial distance of $x/h = 3.75$ in the "Volvo" rig. Symbols, experimental data [20]; Lines, from LES/PDF calculations [11]. Solid line, 30-species mechanism; dashed line, RCCE with $n_{rs} = 11$; dash-dot line, RCCE with $n_{rs} = 16$. (From [11])

As an example of the LES/PDF calculations, figure 3 shows the lateral profile of the mean mass fraction of CO at a distance of $3.75h$ downstream of the flame-holder. The three lines (barely distinguishable) are for different treatments of the propane chemistry: a detailed 30-species mechanism; and two calculations using Rate-Controlled Constrained Equilibrium (RCCE) with 11 and 16 represented species. These calculations demonstrate the capabilities of the LES/PDF approach, and also show that the chemistry can (in this case) be reduced to computational advantage, without significantly compromising accuracy.

Premixed Opposed Jet Flame

The third flame, recently studied using LES/PDF, is the turbulent counter-flow flame studied experimentally by Coriton *et al.* [1]. The flame is formed between two opposed jets. The top jet is a highly turbulent stream of premixed $CH_4/O_2/N_2$ mixture (equivalence ratio 0.85, O_2/N_2 molar ratio 30/70) at $294K$ flowing at $11.2m/s$. The bottom jet is a fully burnt stoichiometric $CH_4/O_2/N_2$ mixture (O_2/N_2 molar ratio 26/74) at $1850K$ flowing at $38.2m/s$.

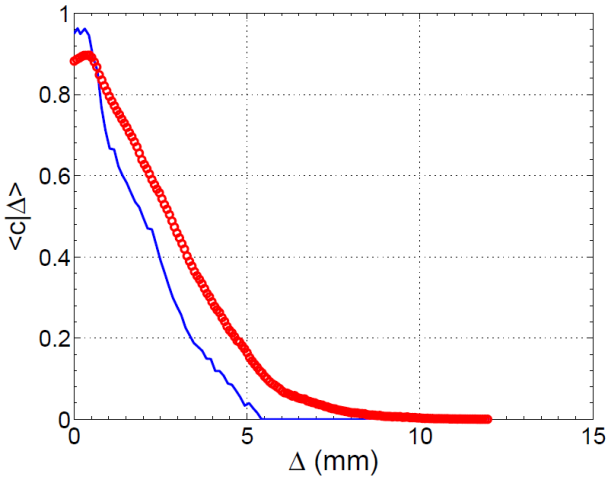

Figure 4: For the turbulent counterflow flame, the mean reaction progress variable conditional on the distance Δ from the GMLI. Symbols, experimental measurements [1]; line, LES/PDF.

In the simulations, the computational domain is taken as a cylindrical region between the two nozzle exits (excluding the region upstream of the nozzle exits) to focus on the combustion region and to make the LES/PDF calculations affordable. A new treatment is developed for the inflow velocity boundary conditions at the nozzle exits to match the mean and r.m.s. velocities and the turbulent length scales in the simulations to those in the experiments.

In the experiment [1], OH imaging is used to define the Gas Mixing Layer Interface (GMLI) as the location on the centerline where the OH concentration first deviates from its value in the hot-product stream. When there is a robust, burning flame, the OH rises steeply at the GMLI as the reaction zone is encountered, and then, after some distance, it decreases as the preheat zone is reached. The reaction progress variable c is defined to be unity between the GMLI and the preheat zone, and zero everywhere else. But when there is local extinction, moving from the product stream towards the reactants, the OH drops, essentially to zero. In this extinguished case, c is defined to be zero everywhere.

Good agreement with the experimental data [1] is observed for unconditional velocity and reaction progress variable statistics. However, it is most informative to look at statistics conditioned on distance from the GMLI. Figure 4 shows the mean of c conditional on the distance Δ from the GMLI. As may be seen, the LES/PDF calculations agree at least qualitatively with the measurements. Note, however, that the quantity $1 - \langle c \,|\, \Delta = 0 \rangle$ is the probability of there being local extinction, and the measured value is about twice that in the LES/PDF.

Furthermore, particle data are analyzed from the PDF code. Figure 5 shows the scatter plot between the mass fractions of CO and CO_2. It can be noted that there is inert mixing between the burnt stream and the partially-burnt reactants (branch between "B" and "E" in figure 5) and on the reactant side, particles align close to the laminar solution, especially at higher temperatures (branch between "R" and "E" in figure 5).

Improved Understanding of the Generalized Langevin Model

The calculations described in the previous section are based

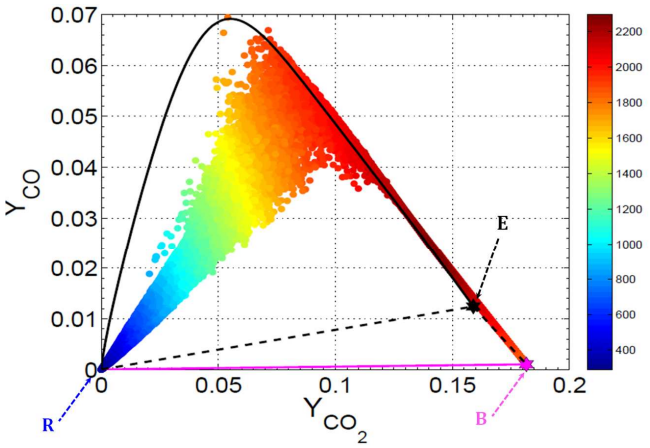

Figure 5: For the turbulent counterflow flame, scatter plot of CO mass fraction vs. CO_2 mass fraction obtained from the PDF code particle data. Dots, particle data from a cylindrical region around the centerline; R, cold, unburnt, premixed reactants; E, equilibirum composition of reactants; B, hot products stream; black solid line, CHEMKIN's OPPDIF laminar solution; black dash lines, mixing line between R & E and B & E; magenta solid line, mixing line between R & B.

on the composition PDF, used in conjunction with LES. In the RANS context, a complete model is provided by the joint PDF of velocity, composition and the turbulence frequency [23, 13]. This joint PDF model has been used extensively to model a broad range of reacting and non-reacting turbulent flows [14, 16].

Here, following [17], we re-examine the turbulence modeling involved in this joint PDF equation. To do so, it is sufficient to consider the velocity PDF in constant-property flow, and (in order to provide scale information) we consider the mean dissipation rate ε to be known.

A stochastic Lagrangian approach is taken to the modeling, in which a stochastic model is used to describe the fluid velocity $\mathbf{U}^*(t)$ following a fluid particle with position $\mathbf{X}^*(t)$, which, by definition evolves according to $d\mathbf{X}^*/dt = \mathbf{U}^*$. The prevalent model for $\mathbf{U}^*$ is the Generalized Langevin Model (GLM) [8, 13]:

$$dU_i^* = -\frac{1}{\rho}\frac{\partial\langle p\rangle}{\partial x_i}\,dt + G_{ij}u_j^*\,dt + (C_0\varepsilon)^{1/2}\,dW_i. \qquad (1)$$

The left-hand side is the infinitesimal increment in velocity over the infinitesimal time interval dt. In the first term on the right-hand side, ρ is the density, $\langle p(\mathbf{x},t)\rangle$ is the mean pressure, and this term ensures that the GLM is consistent with the mean momentum equation (neglecting viscous terms). In the next term, G_{ij} is the GLM model coefficient—the focus of our attention—and $\mathbf{u}^*$ is the fluctuating component of the particle velocity $\mathbf{u}^*(t) \equiv \mathbf{U}^*(t) - \langle \mathbf{U}(\mathbf{X}^*(t),t)\rangle$, where $\langle \mathbf{U}(\mathbf{x},t)\rangle$ is the Eulerian mean velocity field. In the final term, $\mathbf{W}(t)$ is an isotropic Wiener process, whose infinitesimal increments have the properties $\langle d\mathbf{W}\rangle = 0$ and $\langle dW_i dW_j\rangle = dt\,\delta_{ij}$. This diffusion term makes the model consistent with the Kolmogorov hypotheses (when it is examined for time intervals in the inertial subrange), and the model coefficient C_0 is related to a Kolmogorov constant. The coefficient G_{ij} is modeled (locally) as a function of the Reynolds stresses $\langle u_i u_j\rangle$, the mean velocity gradients and ε.

Heretofore, a close connection has not been made between the GLM and the Navier-Stokes equations; and, as a consequence, G_{ij} has not been related to measurable quantities. The reason for this is that the GLM models the fluid acceleration $\mathbf{A} \equiv D\mathbf{U}/Dt$ as white noise, whereas according to the Navier-Stokes equations the acceleration is of course a smooth function.

To remedy these problems, we write the stochastic model for $\mathbf{U}^*(t)$ in the more general form

$$d\mathbf{U}^* = \mathbf{A}^{(p)}\,dt + d\mathbf{U}^{(n)}, \qquad (2)$$

where the drift coefficient $\mathbf{A}^{(p)}$ may depend on $\mathbf{U}^*$ and local statistics obtained from ε and the PDF of velocity (e.g., Reynolds stresses and mean velocity gradients), and hence it is more completely written as $\mathbf{A}^{(p)}(\mathbf{U}^*(t),\mathbf{X}^*(t),t)$.

The random increment $d\mathbf{U}^{(n)}$ is defined by

$$dU_i^{(n)} \equiv -\frac{1}{2}C_0\varepsilon\lambda_{ij}u_j^*\,dt + (C_0\varepsilon)^{1/2}\,dW_i, \qquad (3)$$

where λ_{ij} denotes the i-j component of the inverse of the Reynolds-stress tensor.

This component of the model is specially constructed so that

1. It vanishes in the mean momentum equation derived from Eq. 2
2. It vanishes in the Reynolds-stress equation derived from Eq. 2
3. If the velocity PDF is joint normal, then it also vanishes in the PDF equation derived from Eq. 2.

That is, in Eq. 3, the term in λ_{ij} is designed to nullify the effect of the diffusion term (involving $d\mathbf{W}$) in statistical equations.

By comparing the PDF equation derived from Eq. 2 (with the neglect of the contribution, if any, from $d\mathbf{U}^{(n)}$) to the exact PDF equation, we deduce that, in order for the PDF to evolve correctly, the coefficient $\mathbf{A}^{(p)}$ must satisfy the requirement

$$\mathbf{A}^{(p)}(\mathbf{V},\mathbf{x},t) = \langle \mathbf{A}(\mathbf{x},t)\,|\,\mathbf{U}(\mathbf{x},t) = \mathbf{V}\rangle, \qquad (4)$$

where $\mathbf{V}$ is a sample space variable for velocity. That is, the correct specification of $\mathbf{A}^{(p)}$ is that it is equal to the conditional expectation of the fluid acceleration.

We have thus established a direct connection between the coefficient $\mathbf{A}^{(p)}$ and the Navier-Stokes equations which determine the fluid acceleration $\mathbf{A}$. The superscript "(p)" is used to convey that $\mathbf{A}^{(p)}$ is the "physical" component of acceleration, whereas $d\mathbf{U}^{(n)}$ is the non-physical increment in velocity.

Both $\mathbf{A}$ and $\mathbf{A}^{(p)}$ can be decomposed into their (unconditional) means and their fluctuations, which are denoted $\mathbf{a}$ and $\mathbf{a}^{(p)}$, respectively. The means are simply $-\nabla\langle p\rangle/\rho$, as in the GLM. And then the requirement on $\mathbf{a}^{(p)}$ is simply

$$\mathbf{a}^{(p)}(\mathbf{v},\mathbf{x},t) = \langle \mathbf{a}(\mathbf{x},t)\,|\,\mathbf{u}(\mathbf{x},t) = \mathbf{v}\rangle, \qquad (5)$$

where $\mathbf{u}$ is the velocity fluctuation ($\mathbf{u} \equiv \mathbf{U} - \langle\mathbf{U}\rangle$), and $\mathbf{v} \equiv \mathbf{V} - \langle\mathbf{U}\rangle$ is the corresponding sample-space variable.

There is some evidence from DNS [19] that $\langle \mathbf{a}\,|\,\mathbf{v}\rangle$ can be approximated as being linear in velocity, and hence (similar to GLM) we consider the linear model

$$a_i^{(p)} = G_{ij}^{(p)}v_j, \qquad (6)$$

where the coefficient $G_{ij}^{(p)}$ is to be determined. From Eqs. 4 and 6 we can obtain an explicit expression for $G_{ij}^{(p)}$:

$$G_{ij}^{(p)} = \langle a_i u_k \rangle \lambda_{kj}, \tag{7}$$

where we recall that λ_{ij} denotes the i-j component of the inverse of the Reynolds-stress tensor.

With the advent of particle-tracking velocimetry [12, 5] and tomographic particle image velocimetry (PIV) [4, 2], it is now possible to make measurements of $\langle \mathbf{a} \,|\, \mathbf{v} \rangle$ and $\langle u_i a_j \rangle$, and hence the model coefficients $\mathbf{a}^{(p)}(\mathbf{v})$ and $G_{ij}^{(p)}$ can be obtained directly from laboratory experiments (as they can from DNS).

The Shadow-Position Mixing Model

PDF methods have been most widely used for turbulent reactive flows, especially for turbulent combustion. Following a fluid particle, the composition changes due to just two processes: reaction and molecular diffusion. A great advantage of PDF methods is that reaction can be treated using a detailed chemical mechanism, without further modeling. The effects of molecular diffusion, on the other hand, have to be modeled by means of a "mixing model". Since the 1970s, many mixing models have been proposed, the most widely used having the initials IEM [24], MC [10] and EMST [21].

Recently, Pope [15] introduced the Shadow-Position Mixing Model (SPPM), which is claimed to remove serious deficiencies in previous models. In particular it is (to a good approximation) consistent with Taylor's theory of turbulent dispersion [22], and (also to a good approximation) the mixing is "local" in composition space. It also avoids the "stranding", convergence and transformation problems suffered by EMST, which is the only other "local" model.

According to the SPMM, the composition $\phi^*(t)$ of the particle evolves due to mixing by:

$$\frac{d\phi^*}{dt} = -\frac{c}{T_L}(\phi^* - \langle \phi^* \,|\, \mathbf{R}^*, \mathbf{X}^* \rangle), \tag{8}$$

where c is a model constant, T_L is the Lagrangian velocity integral time scale, and $\mathbf{R}^*(t)$ is a new, non-physical particle property called the "shadow displacement" that evolves by a specified stochastic differential equation. (The shadow position is $\mathbf{Z}^* \equiv \mathbf{X}^* + \mathbf{R}^*$.) Thus, according to the SPMM, the fluid composition relaxes to its local conditional mean, conditional on the shadow displacement.

As with all models, it would be useful to be able to test the SPMM's underlying assumptions using experiments or DNS. A significant difficulty, though, is that the model involves the non-physical (and hence unmeasurable) quantity $\mathbf{R}^*$. Fluid particles can be tracked in DNS, and the equation for $\mathbf{R}^*(t)$ can be integrated, but this requires additional planning, cost and effort.

Here we propose a method to test SPMM which can be employed both in experiments and in DNS post-processing (without the need for particle tracking or other special measures). The method is applicable to two-stream mixing problems in which statistics vary mainly in one predominant direction. This is the case for laboratory jet flames, and for the statistically one-dimensional, temporal jet flames studied in DNS [7].

Considering such flows, we define the mixture fraction ξ to be a conserved scalar that is zero in one stream and unity in the other. The relevant particle properties are: the components of position X^*, velocity U^* and shadow displacement R^* in the direction of variation, and the mixture fraction ξ^*. For the idealized case of statistically-stationary, homogeneous isotropic turbulence with a uniform mean mixture fraction gradient (as considered in [15]), it is found that the variables, U^*, R^* and ξ^* are quite highly correlated. Specifically, in an obvious notation, the correlation coefficients are $\rho_{UR} = -0.58$, $\rho_{U\xi} = -0.55$, and $\rho_{R\xi} = 0.95$. (It is the high correlation between R^* and the composition (here ξ^*) that makes the model "local".)

The proposed method is to generate a *surrogate*, $\bar{R}^*$, for R^*, based on the values of U^* and ξ^*, and to use this surrogate in place of R^* in the SPMM. The surrogate is defined to be the Gaussian random variable with specified values of the correlations coefficients, ρ_{UR} and $\rho_{R\xi}$. Specifically, we specify

$$\rho_{UR} = \rho_{UR}^o \quad \text{and} \quad \rho_{R\xi} = \rho_{R\xi}^o \left(\frac{\rho_{U\xi}}{\rho_{U\xi}^o} \right), \tag{9}$$

where the superscript o denotes the value (given above) for the mean-scalar-gradient case. That is, ρ_{UR} is specified to be the same as in the mean-scalar-gradient case; and $\rho_{R\xi}$ is specified to vary linearly with $\rho_{U\xi}$ and to yield the correct value in the mean-scalar-gradient case. This specification is examined further in the next sub-section, and Eq. 9 is modified to ensure realizability for large values of $|\rho_{U\xi}|$.

The surrogate $\bar{R}^*$ can be written

$$\frac{\bar{R}^*}{\sigma_R} = \alpha \left(\frac{U^* - \langle U \rangle}{\sigma_U} \right) + \beta \left(\frac{\xi^* - \langle \xi \rangle}{\sigma_\xi} \right) + \gamma \eta, \tag{10}$$

where η is a standardized Gaussian random variable (with zero mean and unit variance), σ_U denotes the standard deviation of U^*, *etc.*, and α, β and γ are constants determined by the specified values of ρ_{UR} and $\rho_{R\xi}$, and the normalization condition $\langle (\bar{R}^*/\sigma_R)^2 \rangle = 1$. (Since $\bar{R}^*$ is used only for conditioning, the value of σ_R is immaterial.)

For the case $\rho_{U\xi} = \rho_{U\xi}^o$, the values of the constants are

$$\alpha = -0.077, \quad \beta = 0.91 \quad \text{and} \quad \gamma = 0.30. \tag{11}$$

The large value of β reflects the strong correlation between R^* and ξ^*. The relatively small value of γ shows that a knowledge of U^* and ξ^* reduces the variance of R^* by 70%. It is this observation, that U^* and ξ^* largely determine R^*, that provides grounds for supposing that conditioning on the surrogate $\bar{R}^*$ provides a good approximation to conditioning on R^*.

In order to test the proposed method, the "reactive mixing layer" test case described in Sec.V.A of [15] is performed both with the SPMM (based on R^*), and with the SPPM using the surrogate $\bar{R}^*$, which we denote by S-SPMM. The default values of the SPMM constant $a = 1.0$ is used: the reader is referred to [15] for further information about the test case.

Figures 6 and 7 show the profiles of the standard deviation of mixture fraction σ_ξ and of the scalar flux $\langle u\xi \rangle = \langle U^* \xi^* \rangle$ obtained (at the statistically-stationary state) using both methods. As may be seen, there profiles are very similar, with the deviations at the peak being 5% and 10%, respectively.

This reactive-mixing-layer case is very revealing. It involves two compositions: the mixture fraction ξ, and the product mass fraction Y, which is bounded by zero (corresponding to complete extinction) and the fully-burnt value $Y_f(\xi)$. The known solution is that the fluid is everywhere in the fully burnt state (i.e., $Y^* = Y_f(\xi^*)$), whereas non-local models such as IEM incorrectly predict extinction. The SPMM becomes progressively non-local as the model constant a increases from its minimum

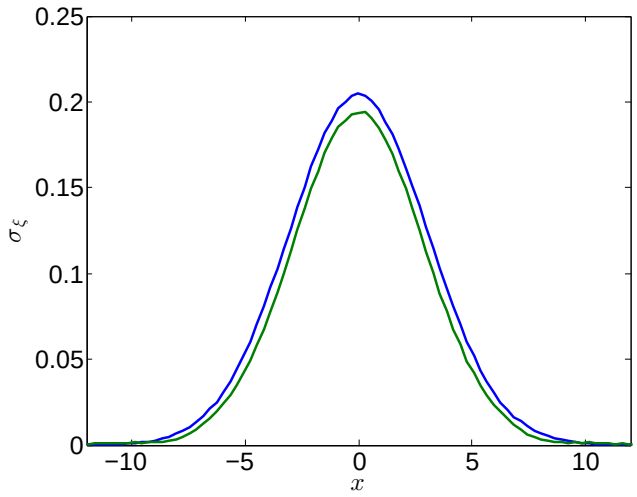

Figure 6: Profile of the standard deviation for the mixture fraction in the reactive-mixing-layer test case in the statistically-stationary state. Blue line - SPMM; Green line - S-SPMM.

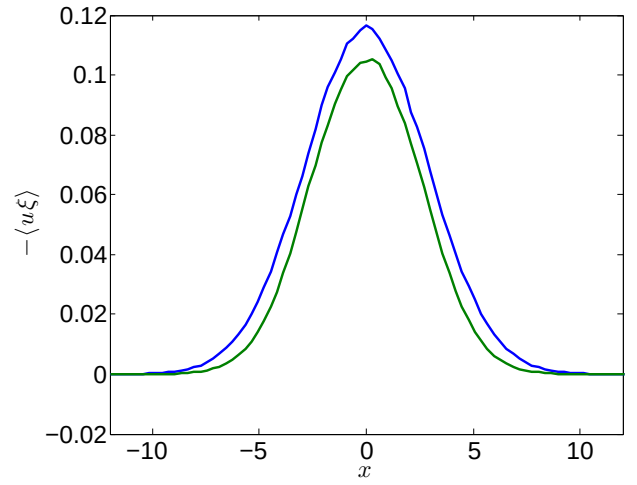

Figure 7: Profile of (minus) the scalar flux for the reactive-mixing-layer test case in the statistically-stationary state. Blue line - SPMM; Green line - S-SPMM.

value ($a_{\min} \approx 0.87$). It is found that both SPMM and S-SPPM yield burning solutions for $a = 1.0$ and 1.1, but extinguished solutions for $a = 1.2$ and higher. Thus the surrogate model captures the essential qualities of SPPM.

The Specification of the R-ξ Correlation Coefficient

We now examine further the specification of the R-ξ correlation coefficient, $\rho_{R\xi}$, given by Eq. 9.

First, shown in figure 8 is a scatter plot of $\rho_{R\xi}$ *vs.* $\rho_{U\xi}$ obtained from the reactive-mixing-layer test case, for all times and for all locations. As may be seen, this amply justifies the linearity assumption embodied in Eq. 9.

Second, we observe that Eq. 9 yields non-realizable values of $\rho_{R\xi}$ (i.e., $|\rho_{R\xi}| > 1$) for values of $|\rho_{U\xi}|$ greater than $\rho_{\rm crit} \equiv |\rho^o_{U\xi}/\rho^o_{R\xi}| \approx 0.58$, and therefore a modification to Eq. 9 is needed to produce an acceptable, realizable model.

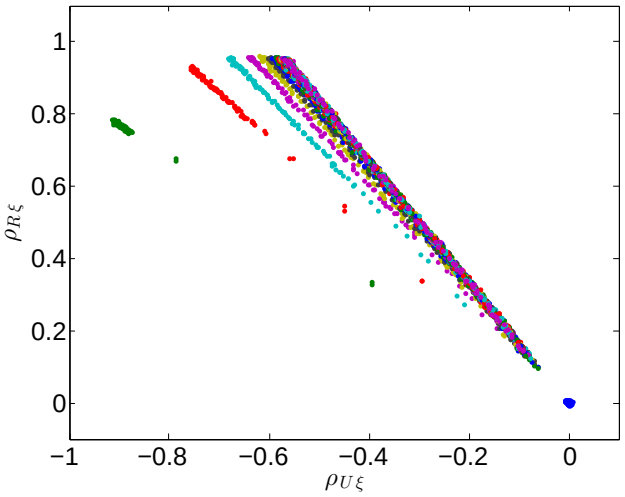

Figure 8: Scatter plot of the R-ξ correlation coefficient *vs.* the U-ξ correlation coefficient for the reactive-mixing-layer test case, for all times and locations color-coded by time. The largest magnitudes are at early times.

For $|\rho_{U\xi}| = \rho_{\rm crit}$, we have $|\rho_{R\xi}| = 1$, and so R^* is completely determined by ξ^*. Equivalently, the conditional variance of R^* (conditional on ξ^*) is zero. For $|\rho_{U\xi}| > \rho_{\rm crit}$ we modify Eq. 9 by specifying $\rho_{R\xi}$ to be as large as possible (in magnitude) while maintaining realizability. With this specification, the variance of R^* conditional on U^* and ξ^* is zero. The corresponding equation for $\rho_{R\xi}$ is obtained from the requirement that the determinant of the correlation-coefficient matrix be zero. The result is:

$$\rho_{R\xi} = \rho_{U\xi}\rho^o_{UR} - \text{sign}(\rho_{U\xi})[(1-\rho^2_{U\xi})(1-\rho^{o2}_{UR})]^{1/2}. \quad (12)$$

Thus, the modified specification, shown in figure 9, is Eq. 9 for $|\rho_{U\xi}| \le \rho_{\rm crit}$, and Eq. 12 for $|\rho_{U\xi}| \ge \rho_{\rm crit}$.

Figure 10 shows the corresponding coefficients in the specification of the Gaussian surrogate by Eq. 10. Note that the coefficient γ of the random term is zero for $|\rho_{U\xi}| \ge \rho_{\rm crit}$.

A Priori Testing of the Shadow Position Mixing Model

We now describe how the surrogate shadow position can be used in the testing of the SPMM. We consider a single location x and time t at which there are many samples (from experiment or DNS) of: the velocity U; the mixture fraction ξ; the composition ϕ (or some components thereof); and, the diffusion term $\mathbf{D}$ in the composition evolution equation. (Note that $\mathbf{D}$ can be extracted from DNS and experiments, either directly, or, for non-reactive compositions, from $\mathbf{D} = D\phi/Dt$.) An estimate of the Lagrangian time scale T_L is also needed.

The testing can be performed following these steps:

1. From the samples of U and ξ, estimate the required statistics, i.e., $\langle U\rangle$, $\langle\xi\rangle$, σ_U, σ_ξ, and $\rho_{U\xi}$.
2. Specify ρ_{UR} and $\rho_{R\xi}$ based on Eqs. 9 and 12, and determine the coefficients α, β and γ in Eq. 10.
3. For each sample, generate the surrogate shadow position $\bar{R}$ using Eq. 10.
4. Evaluate the conditional means $\langle\phi\,|\,\bar{R} = \hat{R}\rangle$, the conditional diffusion $\mathbf{D}_c(\psi,\hat{R}) \equiv \langle\mathbf{D}\,|\,\phi = \psi, \bar{R} = \hat{R}\rangle$ and the S-SPMM model for it $\mathbf{D}_m(\psi,\hat{R}) \equiv (-c/T_L)(\psi - \langle\phi\,|\,\bar{R} = \hat{R}\rangle)$.

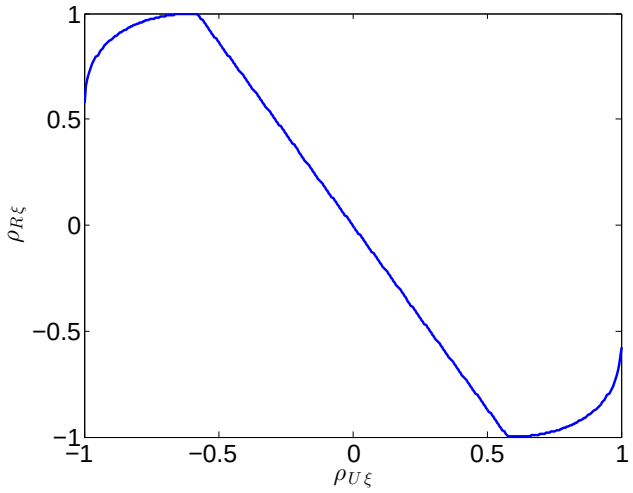

Figure 9: Specification of the R-ξ correlation coefficient as a function of the U-ξ correlation coefficient.

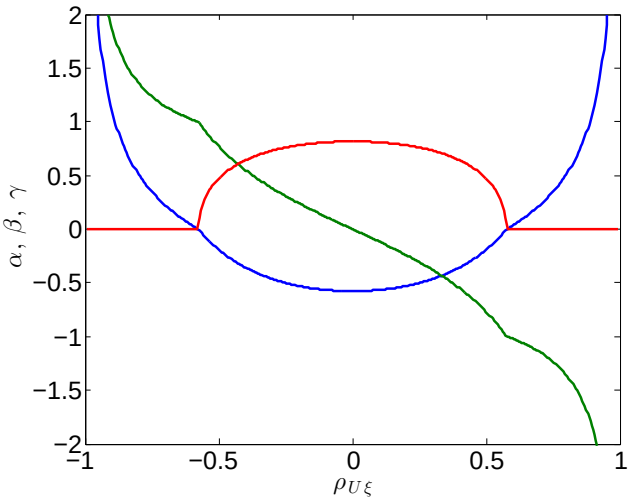

Figure 10: As functions of the U-ξ correlation coefficient, the coefficients in Eq. 10: blue - α; green - β; red - γ.

5. Compare $\mathbf{D}_m(\psi,\hat{R})$ to $\mathbf{D}_c(\psi,\hat{R})$.

6. Form and compare $\langle \mathbf{D}_m(\psi,\bar{R})\rangle$ and $\langle \mathbf{D}_c(\psi,\bar{R})\rangle$, where the averaging is over $\bar{R}$.

Note that the test in 6, which is weaker than that in 5, is sufficient for the composition PDF to evolve correctly.

Conclusions

Good progress is being made in both the application and understanding of PDF methods for turbulent reactive flows. The three LES/PDF calculations reviewed illustrate the capabilities of this methodology to treat challenging turbulent-chemistry interactions in both premixed and non-premixed flames.

For the Generalized Langevin Model (GLM), used to model the fluid particle velocity, a decomposition of the velocity increment (Eq. 2) is given that identifies the physical component of acceleration $\mathbf{A}^{(p)}$. For the model to be exact, this must be equal to the fluid acceleration, in conditional expectation (Eq. 4). With the assumption of linearity made in the GLM, the resulting tensor coefficient $G_{ij}^{(p)}$ is directly related to the velocity-acceleration correlations (by Eq. 7).

A new method is proposed for testing the Shadow-Position Mixing Model (SPMM) in two-stream reactive mixing problems (e.g., jet flames). This is based on the *surrogate* shadow position $\tilde{\mathbf{R}}^*$ defined by Eq. 10, which is determined by the velocity U^* and mixture fraction ξ^*. Since both U^* and ξ^* are measurable, so is the surrogate $\tilde{\mathbf{R}}^*$, whereas the shadow position $\mathbf{R}^*$ is an unmeasurable, non-physical quantity. It is demonstrated that the SPMM using the surrogate (denoted S-SPPM) yields results that are very similar (e.g., to within 10%) to those of the SPMM.

Acknowledgements

This material is based upon work supported by the U.S. Department of Energy, Office of Science, Office of Basic Energy Sciences under Award Number DE-FG02-90 ER14128.

References

[1] Coriton, B., Frank, J. H. and Gomez, A., Effects of strain rate, turbulence, reactant stoichiometry and heat losses on the interaction of turbulent premixed flames with stoichiometric counterflowing combustion product, *Combust. Flame*, **160**, 2013, 2442–2456.

[2] Coriton, B., Steinberg, A. and Frank, J., High-speed tomographic PIV and OH PLIF measurements in turbulent reactive flows, *Exp. Fluids*, **55**, 2014, 1743.

[3] Desjardins, O., Blanquart, G., Balarac, G. and Pitsch, H., High order conservative finite difference scheme for variable density low Mach number turbulent flows, *J. Comput. Phys.*, **227**, 2008, 7125–7159.

[4] Elsinga, G., Wieneke, B., Scarano, F. and van Oudheusden, B., Tomographic particle image velocimetry, *Exp. Fluids*, **41**, 2006, 933–947.

[5] Gerashchenko, S., Sharp, N. S., Neuscamman, S. and Warhaft, Z., Lagrangian measurements of inertial particle accelerations in a turbulent boundary layer, *J. Fluid Mech.*, **617**, 2008, 255–281.

[6] Germano, M., Piomelli, U., Moin, P. and Cabot, W. H., A dynamic subgrid-scale eddy viscosity model, *Phys. Fluids A*, **3**, 1991, 1760–1765.

[7] Hawkes, E. R., Sankaran, R., Sutherland, J. C. and Chen, J. H., Scalar mixing in direct numerical simulations of temporally evolving plane jet flames with skeletal CO/H_2 kinetics, *Proc. Combust. Inst.*, **31**, 2007, 1633–1640.

[8] Haworth, D. C. and Pope, S. B., A generalized Langevin model for turbulent flows, *Phys. Fluids*, **29**, 1986, 387–405.

[9] Haworth, D. C. and Pope, S. B., Transported probability density function methods for Reynolds-averaged and large-eddy simulations, in *Turbulent Combustion*, editors T. Echekki and E. Mastorakos, Springer, 2011, 119–142.

[10] Janicka, J., Kolbe, W. and Kollmann, W., Closure of the transport equation for the probability density function of turbulent scalar fields, *J. Non-Equilib. Thermodyn*, **4**, 1977, 47–66.

[11] Kim, J. and Pope, S. B., Effects of combined dimension reduction and tabulation on the simulations of a turbulent premixed flame using large-eddy simulation/probability density function, *Combust. Theory Modelling*, **18**, 2014, 388–413.

[12] La Porta, A., Voth, G. A., Crawford, A. M., Alexander, J. and Bodenschatz, E., Fluid particle accelerations in fully developed turbulence, *Nature*, **409**, 2001, 1017–1019.

[13] Pope, S. B., *Turbulent Flows*, Cambridge University Press, Cambridge, 2000.

[14] Pope, S. B., Simple models of turbulent flows, *Phys. Fluids*, **23**, 2011, 011301.

[15] Pope, S. B., A model for turbulent mixing based on shadow-position conditioning, *Phys. Fluids*, **25**, 2013, 110803.

[16] Pope, S. B., Small scales, many species and the manifold challenges of turbulent combustion, *Proc. Combust. Inst.*, **34**, 2013, 1–31.

[17] Pope, S. B., The determination of turbulence-model statistics from the velocity-acceleration correlation, *J. Fluid Mech.*, (submitted).

[18] Popov, P. and Pope, S. B., Implicit and explicit schemes for mass consistency preservation in hybrid particle/finite-volume algorithms for turbulent reactive flows, *J. Comput. Phys.*, **257**, 2014, 3652–373.

[19] Sawford, B. L. and Yeung, P. K., Eulerian acceleration statistics as a discriminator between Lagrangian stochastic models in uniform shear flow, *Phys. Fluids*, **12**, 2000, 2033–2045.

[20] Sjunnesson, A., Olovsson, S. and Sjöblom, B., Validation rig — a tool for flame studies, in *International Symposium on Air Breathing Engines*, Georgia Institute of Technology, Nottingham, England, 1991, 385–393, 385–393.

[21] Subramaniam, S. and Pope, S. B., A mixing model for turbulent reactive flows based on Euclidean minimum spanning trees, *Combust. Flame*, **115**, 1998, 487–514.

[22] Taylor, G. I., Diffusion by continuous movements, *Proc. Lond. Math. Soc.*, **20**, 1921, 196–212.

[23] Van Slooten, P. R., Jayesh and Pope, S. B., Advances in PDF modeling for inhomogeneous turbulent flows, *Phys. Fluids*, **10**, 1998, 246–265.

[24] Villermaux, J. and Devillon, J. C., Représentation de la coalescence et de la redispersion des domaines de ségrégation dans un fluide par un modèle d'interaction phénoménologique, in *Proceedings of the 2nd International Symposium on Chemical Reaction Engineering*, Elsevier, New York, 1972, 1–13, 1–13.

[25] Viswanathan, S., Wang, H. and Pope, S. B., Numerical implementation of mixing and molecular transport in LES/PDF studies of turbulent reacting flows, *J. Comput. Phys.*, **230**, 2011, 6916–6957.

[26] Wang, H. and Pope, S. B., Large eddy simulation/probability density function modeling of a turbulent $CH_4/H_2/N_2$ jet flame, *Proc. Combust. Inst.*, **33**, 2011, 1319–1330.

[27] Yang, Y., Wang, H., Pope, S. B. and Chen, J. H., Large-eddy simulation/probability density function modeling of a non-premixed CO/H_2 temporally evolving jet flame, *Proc. Combust. Inst.*, **34**, 2013, 1241–1249.